Analytic models of distributed acoustic sensing data for straight and helical fibre

Heather K. Hardeman-Vooys and Michael P. Lamoureux

ABSTRACT

We discuss the process of acquiring seismic data using distributed acoustic sensing. We then describe the analytic model used to depict this process mathematically. We find the strain tensor for the full-waveform by separating the problem in to the case for the P-wave strain tensor and the S-wave strain tensor. We show examples of the model for the P-wave response of the fibre in two different media. We compare the results of the S-wave response for helical and straight fibre. Finally, we examine the full-waveform response of the fibre and consider the results using different gauge lengths.

INTRODUCTION

Distributed acoustic sensing is a relatively new way to gather seismic data; it uses fibre optic cables and laser interferometry for data acquisition. Unlike geophones, fibre is inexpensive and provides a continuous receiver which can be oriented in many different configurations. Given its low cost, fibre optic cables can be installed permanently in seismic acquisition projects. Fibre-optic cables and DAS can be employed for more than just seismic acquisition. It is often installed in construction projects in cities. Such installations provide the ability to monitor roads and city transportation using an interrogator.

Given the abundance of uses for fibre-optic cables and DAS, modeling such data is of interest. In this paper, we model DAS data analytically, using the true seismic wavefield for constant velocity in 3D, with an arbitrary path for the placement of the DAS fibre. The advantage of this approach is that we can rapidly simulate the true fibre reponse in 3D, in a variety of fibre trials, since we only need to compute data at points on the fibre. This is much faster than calculating a 3D finite difference simulation of a seismic wavefield. It also provides a useful comparison to other simulation methods, such as the work of (Eaid et al., 2017). The analytic method also allows an explicit separation of the P- and S-wave responses for the fibre. In the following section, we describe the problem of acquiring seismic data using distributed acoustic sensing. In the remaining sections of the paper, we look at examples of the model used for the P-wave in two different media. We compare the results of the S-wave response of straight and helical fibre. Then, we show the full response of the straight fibre given different gauge lengths.

ACQUISITION USING DISTRIBUTED ACOUSTIC SENSING AND FIBRE OPTIC CABLES

In seismic acquisition, a fibre optic cable is installed in a specific configuration. In this project, we consider a fibre optic cable buried horizontally 10 meters beneath the earth's surface over a distance of 100 m. Fig. 1 is an example of full-waveform response of the fibre acquired from this formation.

To form the data set in Fig. 1, a source is positioned in the centre of the fibre at the

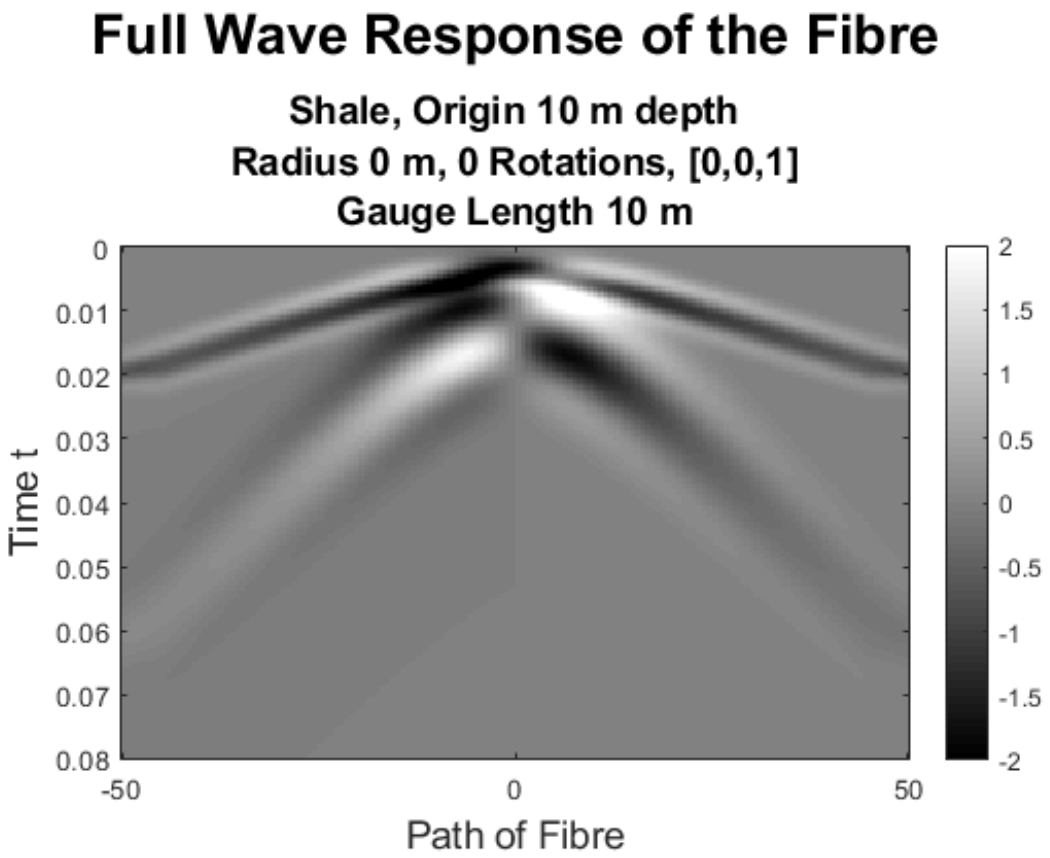

FIG. 1. Full-waveform response of the straight fibre in Shale when the gauge length is set to 10m.

Earth's surface. Once the source detonates, it sends waves into the ground. When these waves hit the fibre, they stretch and strain the fibre optic cable. The strain on the fibre is recovered by an interrogator attached to the cable using a laser pulse that interacts with imperfections in the cable.

Fig. 2 depicts the description of DAS acquistion. A source is represented by a red 'x'. The blue line represents the fibre 10 m deep. The green half-sphere describes the wave moving away from the source. The receiver is the point where the wave hits the fibre for that portion of the wave. We see that the wave hits two points on the fibre for this portion of the wave. As the wave made by the source moves further from the origin, the wave hits more of the fibre until the fibre ends or the wave dissipates.

In the case of constant velocity, seismic waves move through the earth's subsurface in a spherical shape. In fact, an exercise in calculus shows that the Laplace operator can be considered in terms of radial solutions:

$$\Delta\eta = \partial_r^2\eta + \frac{2}{r}\partial_r\eta \tag{1}$$

where $\eta = \eta(r)$ depends only on radial distance. In this report, we utilize the solution u of the acoustic wave equation written in terms of the P-wave and S-wave components

$$u = \nabla\Phi + \nabla \times \Psi \tag{2}$$

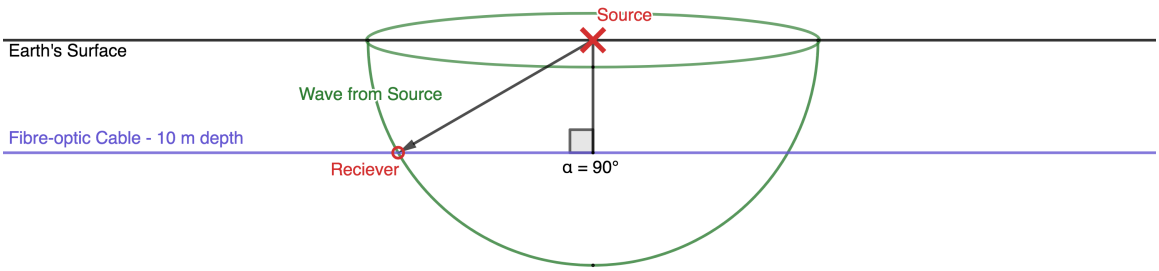

FIG. 2. Physical Model

which we derive from the wave equation using the Helmholtz Decomposition Theorem (Aki and Richards, 2002). Since derivatives are additive, the P-wave and S-wave components satisfy the wave equation and thus can be written using radial solutions. We will use this fact later when we begin creating our model.

In this experiment, the strain is the measure of how much the wave moves the fibre. The equation for strain is defined as follows:

$$\epsilon_{ij} = \frac{1}{2}(\partial_i u_j + \partial_j u_i). \tag{3}$$

The strain ϵ is a symmetric 3×3 matrix with three eigenvectors and three eigenvalues which describe how much the material moves in each of three orthogonal directions.

In order to recover the response of the fibre in this paper, we consider the fact that the wave hits the fibre at any given point $\mathbf{p}(s_0)$ where $\mathbf{p}$ is the path of the fibre. At some point in space, the fibre-optic cable has a tangent vector $\mathbf{T_p} = \mathbf{T_p}(x, y, z)$, which we assume is normalized. The amount of stretching at this point is given by the product of the strain matrix with the tangent vector. Thus, we can determine the strain at this point on $\mathbf{p}$ by the following equation:

$$A(s,t) = \mathbf{T_p}(s)\epsilon(\sqrt{\mathbf{p}(s)})\mathbf{T_p}'(s), \tag{4}$$

where the matrix $\epsilon(\sqrt{\mathbf{p}(s)})$ is the strain at the point s on the path $\mathbf{p}$ of the fibre which is a distance $r = \sqrt{\mathbf{p}(s)}$ away from the source at the origin.

To model the problem described above, we need to solve for the strain tensor. Using Eqn. 2, we solve for the strain produced by the full-waveform. Recall

$$\epsilon_{ij} = \frac{1}{2}(\partial_i u_j + \partial_j u_i) \tag{5}$$

is the ij-th element of the strain tensor. Then, we have

$$\epsilon_{ij} = \frac{1}{2}(\partial_i u_j + \partial_j u_i) \tag{6}$$
$$= \frac{1}{2}(\partial_i((\nabla\Phi)_j + (\nabla \times \Psi)_j) + \partial_j((\nabla\Phi)_i + (\nabla \times \Psi)_i)) \tag{7}$$
$$= \frac{1}{2}(\partial_i(\nabla\Phi)_j + \partial_i(\nabla \times \Psi)_j + \partial_j(\nabla\Phi)_i + \partial_j(\nabla \times \Psi)_i) \tag{8}$$
$$= \frac{1}{2}(\partial_i(\nabla\Phi)_j + \partial_j(\nabla\Phi)_i) + \frac{1}{2}(\partial_i(\nabla \times \Psi)_j + \partial_j(\nabla \times \Psi)_i) \tag{9}$$
$$= \epsilon^{\Phi}_{ij} + \epsilon^{\Psi}_{ij} \tag{10}$$

which implies that the full-waveform strain tensor is the sum of the P-wave strain tensor (ϵ^{Φ}) and the S-wave strain tensor (ϵ^{Ψ}).

Solving for both tensors separately, we start with the P-wave strain tensor ϵ^{Φ}. For the purposes of this paper, we work with the scalar potential

$$\Phi(x, y, z, t) = \frac{1}{r} e^{-(r-\alpha t)^2/\sigma^2} \tag{11}$$

where σ is a typical wavelength and $r = \sqrt{x^2 + y^2 + z^2}$. The Gaussian will give a radial solution to the wave equation.

Taking the gradient of Φ, we find that

$$\nabla\Phi = \left(\frac{\partial}{\partial x}\frac{1}{r}F(r - \alpha t), \frac{\partial}{\partial y}\frac{1}{r}F(r - \alpha t), \frac{\partial}{\partial x}\frac{1}{r}F(r - \alpha t)\right) \tag{12}$$

where $F = \exp(-r^2/\sigma^2)$. Given that F is a Gaussian, we solve for one component and the rest follow similarly. For the first component, we have

$$\frac{\partial}{\partial x}\frac{1}{r}F(r - \alpha t) = \left(-\frac{1}{r^2}F + \frac{1}{r}F'\right)\frac{\partial r}{\partial x} \tag{13}$$
$$= \left(-\frac{1}{r^2}F + \frac{1}{r}F'\right)\frac{x}{r} \tag{14}$$
$$= -\frac{x}{r^2}\left(\frac{1}{r} + 2\frac{(r - \alpha t)}{\sigma^2}\right)F(r - \alpha t) \tag{15}$$

since F is a Gaussian of width σ. Hence, the gradient of Φ is

$$\nabla\Phi = (x, y, z)\frac{1}{r^2}\left(\frac{1}{r} + 2\frac{(r - \alpha t)}{\sigma^2}\right)F(r - \alpha t) \tag{16}$$
$$= (x, y, z)G(r, t) \tag{17}$$

where

$$G(r, t) = -\frac{1}{r^2}\left(\frac{1}{r} + 2\frac{(r - \alpha t)}{\sigma^2}\right)F(r - \alpha t). \tag{18}$$

Then, we find the strain of $\nabla\Phi$ by for each component separately. Thus,

$$\epsilon^{\Phi}_{11} = \frac{1}{2}(\partial_1(\nabla\Phi)_1 + \partial_1(\nabla\Phi)_1) \tag{19}$$
$$= \frac{\partial(\nabla\Phi)_1}{\partial x} \tag{20}$$
$$= \frac{\partial}{\partial x} xG(r,t) \tag{21}$$
$$= G + x\frac{\partial G}{\partial x} \tag{22}$$
$$= G + x\frac{\partial G}{\partial r}\frac{\partial r}{\partial x} \tag{23}$$
$$= G + \frac{x^2}{r}\frac{\partial G}{\partial r}. \tag{24}$$

Similarly,

$$\epsilon^{\Phi}_{22} = G + \frac{y^2}{r}\frac{\partial G}{\partial r}, \text{ and} \tag{25}$$
$$\epsilon^{\Phi}_{33} = G + \frac{z^2}{r}\frac{\partial G}{\partial r}. \tag{26}$$

For the off-diagonal terms, we compute

$$\epsilon^{\Phi}_{12} = \frac{1}{2}(\partial_1(\nabla\Phi)_2 + \partial_2(\nabla\Phi)_1) \tag{27}$$
$$= \frac{1}{2}\left(\frac{\partial}{\partial x} yG + \frac{\partial}{\partial y} xG\right) \tag{28}$$
$$= \frac{1}{2}\left(y\frac{\partial G}{\partial x} + x\frac{\partial G}{\partial y}\right) \tag{29}$$
$$= \frac{1}{2}\left(\frac{xy}{r}\frac{\partial G}{\partial r} + \frac{xy}{r}\frac{\partial G}{\partial r}\right) \tag{30}$$
$$= \frac{xy}{r}\frac{\partial G}{\partial r}. \tag{31}$$

By symmetry, we get

$$\epsilon^{\Phi}_{21} = \frac{xy}{r}\frac{\partial G}{\partial r}. \tag{32}$$

Similarly, we find

$$\epsilon^{\Phi}_{13} = \epsilon^{\Phi}_{31} = \frac{xz}{r}\frac{\partial G}{\partial r}, \text{ and} \tag{33}$$
$$\epsilon^{\Phi}_{23} = \epsilon^{\Phi}_{32} = \frac{yz}{r}\frac{\partial G}{\partial r}. \tag{34}$$

Therefore, the strain tensor ϵ^{Φ} is

$$\epsilon^{\Phi} = GI + \frac{1}{r}\frac{\partial G}{\partial r}\mathbf{R} \tag{35}$$

where I is the 3×3 identity matrix and

$$\mathbf{R} = \begin{bmatrix} x^2 & xy & xz \\ xy & y^2 & yz \\ xz & yz & z^2 \end{bmatrix}. \tag{36}$$

Using standard calculus and algebraic techniques, we find that

$$\frac{\partial G}{\partial r} = \left(\frac{2}{\sigma^2 r^2} - \frac{6(r-\alpha t)}{\sigma^2 r^3} - \frac{4(r-\alpha t)^2}{\sigma^4 r^2} - \frac{3}{r^4} \right) F(r-\alpha t). \tag{37}$$

For the S-wave strain tensor, ϵ^{Ψ}, we define the vector potential as

$$\Psi(x,y,z,t) = \frac{1}{r} F(r-\alpha t)[A_x, A_y, A_z], \tag{38}$$

where $r = \sqrt{x^2+y^2+z^2}$ and $A_x, A_y, A_z \in \mathbb{R}$. As with Φ, this choice of Ψ follows from the discussion on radial solutions seen earlier in the report. We compute the curl

$$\nabla \times \Psi = \begin{bmatrix} \widehat{i} & \widehat{j} & \widehat{k} \\ \frac{\partial}{\partial x} & \frac{\partial}{\partial y} & \frac{\partial}{\partial z} \\ \Psi_1 & \Psi_2 & \Psi_3 \end{bmatrix} \tag{39}$$

$$= \left(\frac{\partial \Psi_3}{\partial y} - \frac{\partial \Psi_2}{\partial z}, \frac{\partial \Psi_1}{\partial z} - \frac{\partial \Psi_3}{\partial x}, \frac{\partial \Psi_2}{\partial x} - \frac{\partial \Psi_1}{\partial y} \right). \tag{40}$$

Computing the partial derivatives of each $(\nabla \times \Psi)_n$ for $n = 1, 2, 3$, we have

$$(\nabla \times \Psi)_1 = \frac{\partial \Psi_3}{\partial y} - \frac{\partial \Psi_2}{\partial z} \tag{41}$$

$$= G(r,t) A_z y - G(r,t) A_y z \tag{42}$$

$$= G(r,t)(A_z y - A_y z) \tag{43}$$

$$(\nabla \times \Psi)_2 = \frac{\partial \Psi_1}{\partial z} - \frac{\partial \Psi_3}{\partial x} \tag{44}$$

$$= G(r,t) A_x z - G(r,t) A_z x \tag{45}$$

$$= G(r,t)(A_x z - A_z x) \tag{46}$$

$$(\nabla \times \Psi)_3 = \frac{\partial \Psi_2}{\partial x} - \frac{\partial \Psi_1}{\partial y} \tag{47}$$

$$= G(r,t) A_y x - G(r,t) A_x y \tag{48}$$

$$= G(r,t)(A_y x - A_x y). \tag{49}$$

Hence, the curl is

$$\nabla \times \Psi = G(r,t)[\mathbf{X}, \mathbf{Y}, \mathbf{Z}] \tag{50}$$

where

$$\mathbf{X} = A_z y - A_y z, \tag{51}$$

$$\mathbf{Y} = A_x z - A_z x, \text{ and} \tag{52}$$

$$\mathbf{Z} = A_y x - A_x y. \tag{53}$$

To solve for each component of the S-wave strain ϵ^{Ψ}, we have

$$\epsilon_{11} = \frac{\partial(\nabla \times \Psi)_1}{\partial x} = \frac{\partial}{\partial x}(G(r,t)\mathbf{X}) \tag{54}$$

$$= \left(\frac{x}{r}\frac{\partial G}{\partial r}\mathbf{X} - G\frac{\partial \mathbf{X}}{\partial x}\right) \tag{55}$$

$$= \frac{x}{r}\frac{\partial G}{\partial r}\mathbf{X} \tag{56}$$

since

$$\frac{\partial \mathbf{X}}{\partial x} = \frac{\partial}{\partial x}(A_z y - A_y z) = 0. \tag{57}$$

By a similar argument,

$$\epsilon_{22} = \frac{y}{r}\frac{\partial G}{\partial r}\mathbf{Y}, \text{ and} \tag{58}$$

$$\epsilon_{33} = \frac{z}{r}\frac{\partial G}{\partial r}\mathbf{Z}. \tag{59}$$

For the off-diagonal cases, we have symmetry so we only need to find ϵ_{12}, ϵ_{13}, and ϵ_{23}. Then, we have

$$\epsilon_{12} = \frac{1}{2}\left(\frac{\partial(\nabla \times \Psi)_2}{\partial x} + \frac{\partial(\nabla \times \Psi)_1}{\partial y}\right) \tag{60}$$

$$= \frac{1}{2}\left[\left(\frac{x}{r}\frac{\partial G}{\partial r}\mathbf{Y} - GA_z\right) + \left(\frac{y}{r}\frac{\partial G}{\partial r}\mathbf{X} + GA_z\right)\right] \tag{61}$$

$$= -\frac{1}{2}\frac{1}{r}\frac{\partial G}{\partial r}(x\mathbf{Y} + y\mathbf{X}). \tag{62}$$

Using a similar method, we get that

$$\epsilon_{13} = \frac{1}{2}\frac{1}{r}\frac{\partial G}{\partial r}(x\mathbf{Z} + z\mathbf{X}), \text{ and} \tag{63}$$

$$\epsilon_{23} = \frac{1}{2}\frac{1}{r}\frac{\partial G}{\partial r}(y\mathbf{Z} + z\mathbf{Y}). \tag{64}$$

giving the complete strain equation ϵ as

$$\epsilon = \frac{1}{2}\frac{1}{r}\frac{\partial G}{\partial r}\begin{bmatrix} 2x\mathbf{X} & x\mathbf{Y} + y\mathbf{X} & x\mathbf{Z} + z\mathbf{X} \\ y\mathbf{X} + x\mathbf{Y} & 2y\mathbf{Y} & y\mathbf{Z} + z\mathbf{Y} \\ z\mathbf{X} + x\mathbf{Z} & z\mathbf{Y} + y\mathbf{Z} & 2x\mathbf{X} \end{bmatrix}. \tag{65}$$

We compute the strain tensor ϵ for the full-waveform to be

$$\epsilon = \epsilon^{\Phi} + \epsilon^{\Psi} \tag{66}$$

$$= G_{\Phi} I + \frac{1}{r}\frac{\partial G_{\Phi}}{\partial r}R_{\Phi} + \frac{1}{2}\frac{1}{r}\frac{\partial G_{\Psi}}{\partial r}R_{\Psi} \tag{67}$$

where G_Φ and G_Ψ signify whether to use the P-wave (Φ) or S-wave (Ψ) velocity for the function G.

Now that we have calculated the strain tensor results for the P-wave, S-wave, and full-waveform, we can consider examples for P-wave and S-wave separately as well as the full-waveform. During these examples, we will also compare responses given different minerals, discuss the difference between straight and helical fibre, and examine the effect of varying the gauge length.

EXAMPLES

In this section, we consider three examples. The first example looks at the P-wave response of a straight fibre for two different velocities. We will see the effect that different minerals have on the response of the fibre. The second example compares the S-wave response of the straight and helical fibre. We examine the differences between the two cases from the fibre in one mineral. In the final example, we analyze the results of the full-wave response of the fibre in one mineral given different gauge lengths.

P-wave example

We begin by a quick study of the fibre's response given different media. Using the P-wave as an example, we examine two different media: saturated shale and limestone.

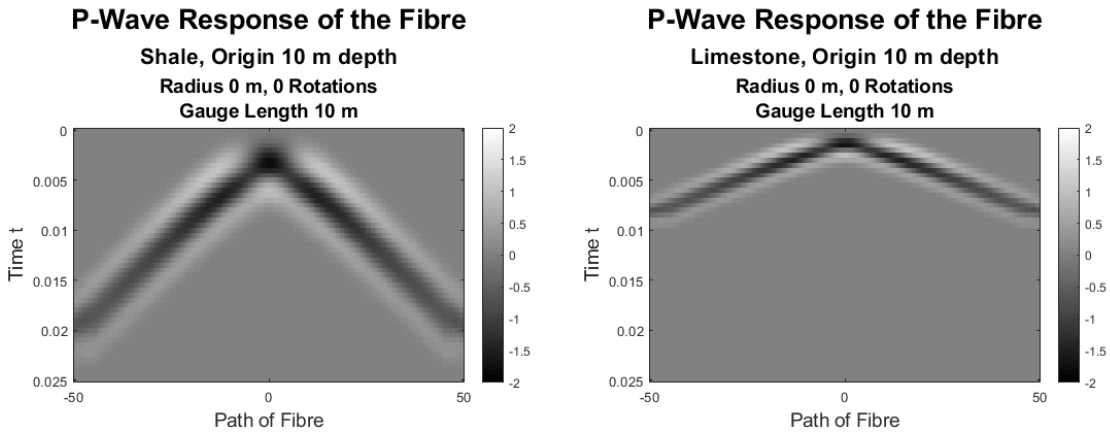

FIG. 3. The P-wave response of the straight fibre in (left) saturated shale - 2500 m/s and (right) limestone - 6000 m/s

Fig. 3 gives the results of the straight fibre's response for the P-wave in saturated shales (left) and limestone (right). Both responses are hyperbolic in shape; however, the hyperbola has a steeper slope in saturated shales as opposed to the more shallow slope of the limestone. This follows physically since the wave moves faster in limestone than it does in shale.

The hyperbola for both the saturated shales response and the limestone response also has three distinct color changes in amplitude. The changes shows the stretch and strain of the fibre as the wave passes over the fibre-optic cable in time.

S-wave example

For the S-wave response, we examine the differences between straight fibre and helical fibre. For the helical fibre, the setup remains the same as the straight fibre, i.e. laid horizontally 10 meters deep; however, fibre forms a helix of with radius 1 cm and has 10 rotations per meter. Over the 100 meter distance we consider in the experiment, the fibre has 1000 rotations. We only look at the results in saturated shales. Given the results of the P-wave example, the S-wave response for limestone would be a shallow hyperbola in comparison to the steeper hyperbola we will see given by the saturate shales since the velocity of the S-wave for limestone is 3300 m/s as opposed to the 800 m/s velocity of the S-wave for saturated shales. As with the P-wave example, we use the max velocity of the S-wave for the media as given in (Bourbié et al., 1987).

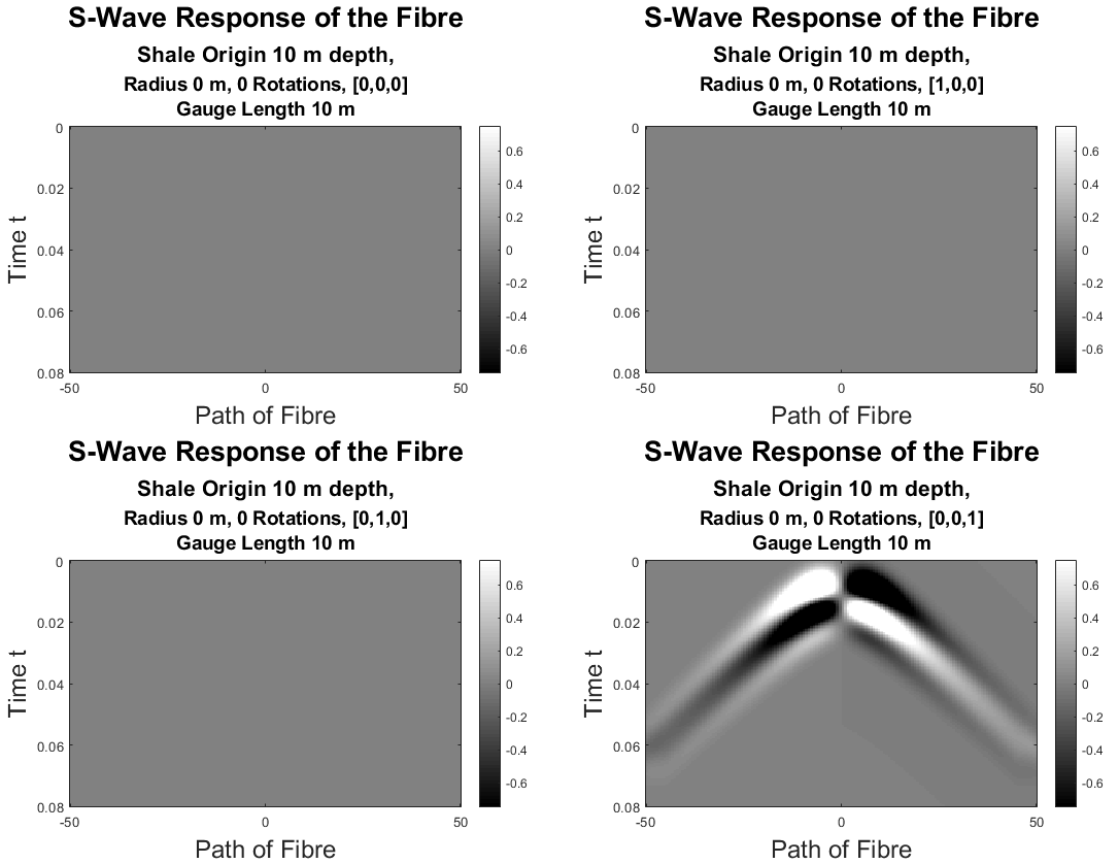

FIG. 4. The S-wave response of the straight fibre in saturated shale when (top left) A = [0,0,0], (top right) A = [1,0,0], (bottom left) A = [0,1,0], and (bottom right) A = [0,0,1]

Fig. 4 and 5 show the S-wave response of the straight fibre in saturated shales for different vectors A. When $A = [0, 0, 0]$, the S-wave response is understandably 0. For $A = [1, 0, 0]$, $A = [0, 1, 0]$, and $A = [1, 1, 0]$, the fibre gives no response; yet, when $A = [0, 0, 1]$, $A = [0, 1, 1]$, $A = [1, 0, 1]$ and $A = [1, 1, 1]$, the straight fibre does detect stress and strain. This result suggests that the straight fibre does not detect stress or strain in the x- and y- directions.

Visually, the results for $A = [0, 0, 1]$ look brighter than the results for the other vec-

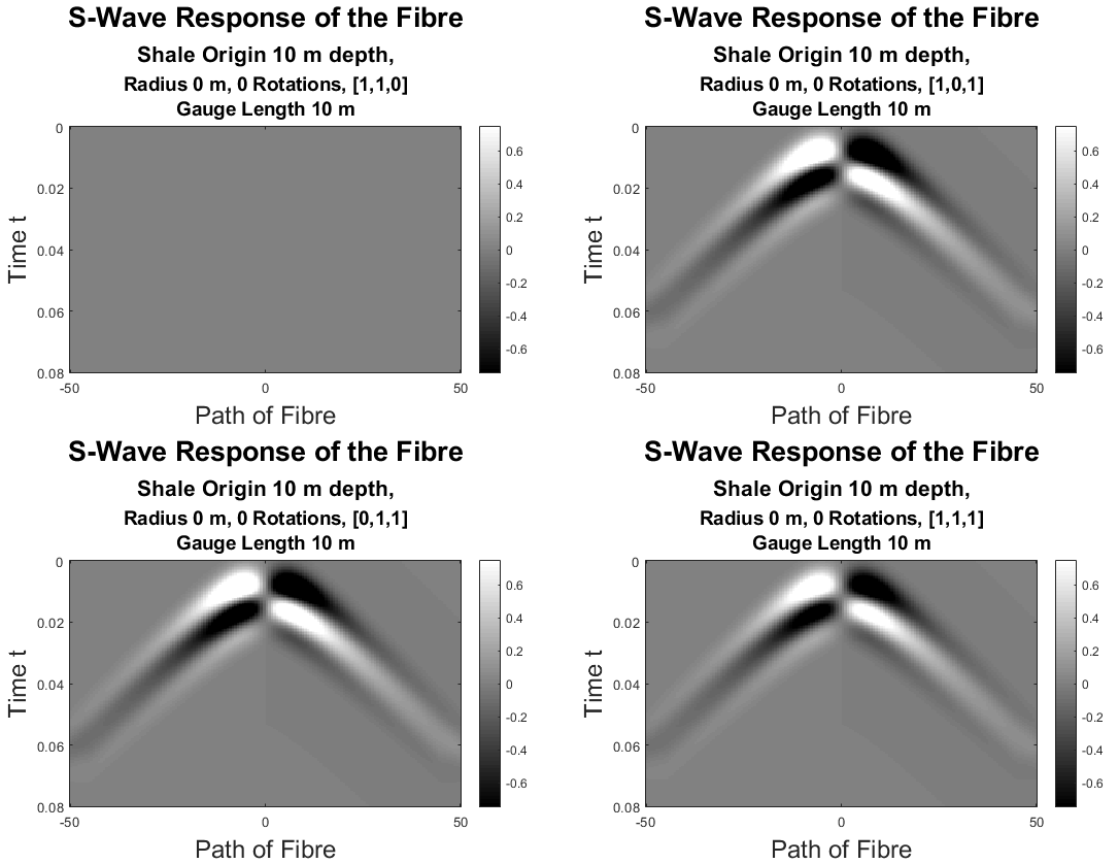

FIG. 5. The S-wave response of the straight fibre in saturated shale when (top left) A = [1,1,0], (top right) A = [1,0,1], (bottom left) A = [0,1,1], and (bottom right) A = [1,1,1]

tors A with non-zero z components. A comparison shows a difference ranging between -0.6167 and 0.6173 for the responses when $A = [0, 1, 1]$ and $A = [1, 0, 1]$ whereas the difference ranges between -0.8900 and 0.8907 for the response when $A = [1, 1, 1]$. These results imply that having both $x-$ and $y-$ components be non-zero dampens the response of the fibre more than having only one of the $x-$ and $y-$ components be non-zero. Furthermore, comparing the results from $A = [0, 1, 1]$ and $A = [1, 0, 1]$ gives a difference of 0. It is an interesting question as to what the physical reason is for the result that there is no difference between the case when $A = [0, 1, 1]$ and $A = [1, 0, 1]$.

It is interesting to note that the addition of a non-zero $x-$ or $y-$ component to the vector A that has a non-zero z-component ($A = [0, 1, 1]$, $A = [1, 0, 1]$, $A = [1, 1, 1]$) results in a different response when having only a non-zero $x-$ or $y-$ component ($A = [1, 0, 0]$,$A = [0, 1, 0]$) resulted in no response from the fibre. Potentially, these are the vectors where the straight fibre is perpendicular to the source for the S-wave.

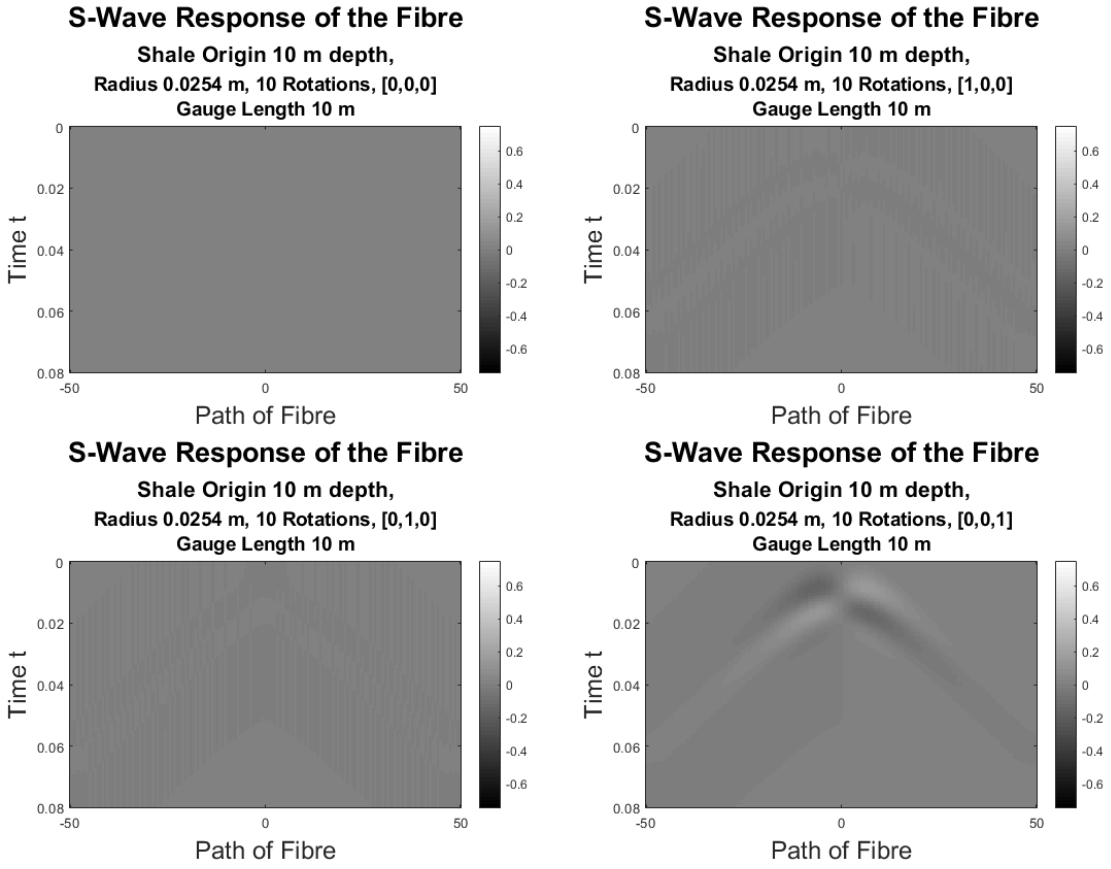

FIG. 6. The S-wave response of the helical fibre in saturated shale when (top left) A = [0,0,0], (top right) A = [1,0,0], (bottom left) A = [0,1,0], and (bottom right) A = [0,0,1]

Fig. 6 and 7 show the S-wave response of the helical fibre in saturated shale for different vectors A. As with the case for the straight fibre, the vector $A = [0, 0, 0]$ provides a response of 0; but, the result for vectors $A = [1, 0, 0]$ and $A = [0, 1, 0]$ shows the fibre detects some strain from the wave. While it is not a lot, it is still more than the straight fibre provided. Table 1 shows the range of the amplitude for the straight and helical fibre response at different vectors A.

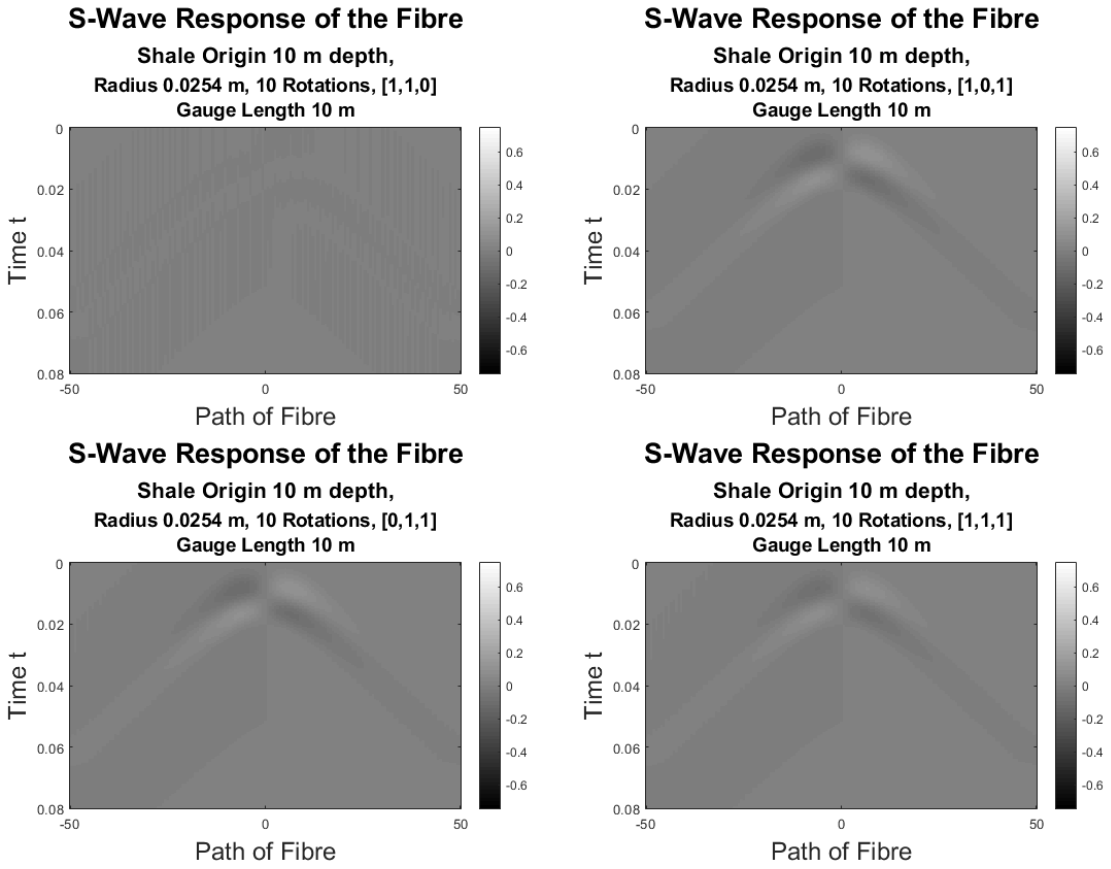

FIG. 7. The S-wave response of the helical fibre in saturated shale when (top left) A = [1,1,0], (top right) A = [1,0,1], (bottom left) A = [0,1,1], and (bottom right) A = [1,1,1]

Table 1. Amplitude range of the straight and helical fibre response for different vectors A

Vector A	Straight Fibre Range	Helical Fibre Range
$[0,0,0]$	0	0
$[1,0,0]$	0	$(-0.0063, 0.0062)$
$[0,1,0]$	0	$(-0.0046, 0.0040)$
$[0,0,1]$	$(-2.1057, 2.1075)$	$(-0.1632, 0.1642)$
$[1,1,0]$	0	$(-.0069, 0.0049)$
$[0,1,1]$	$(-1.4890, 1.4902)$	$(-0.1158, 0.1160)$
$[1,0,1]$	$(-1.4890, 1.4902)$	$(-0.1156, 0.1163)$
$[1,1,1]$	$(-1.2157, 1.2168)$	$(-0.0948, 0.0951)$

Besides producing a response for vectors $A = [1, 0, 0]$, $A = [0, 1, 0]$, and $A = [1, 1, 0]$ unlike the straight fibre's response, the helical fibre produces different responses for the vectors $A = [0, 1, 1]$ and $A = [1, 0, 1]$ whereas the straight fibre's response was the same for both vectors. It is also interesting to note that for both the straight and helical fibre responses, vector $A = [0, 0, 1]$ has an amplitude almost twice the size of the amplitude found in $A = [1, 1, 1]$. With regards to the dampened amplitude of the helical fibre, we see that the amplitude of the straight fibre is about 13 times the size of the amplitude of the helical fibre's response for vectors $A = [0, 0, 1]$, $A = [0, 1, 1]$, $A = [1, 0, 1]$, and $A = [1, 1, 1]$.

While the response is dampened for helical fibre, more vectors A provide a response for the helical fibre which supports the use of helical fibre in acquisition as it is more sensitive to strain in more than just the z-direction. Not only is the helical fibre more sensitive, but the data set for the helical fibre is actually larger than the straight fibre. For all vectors A, the data set of the straight fibre is 500×152 (Time$t \times$ Path of Fibre$\mathbf{p}(s)$) whereas the data set of the helical fibre is 500×157. The difference results from the fact that the sample points are taken along the helical distance of the fibre. Since the sample points are $2/3$ m apart, the straight fibre only gives sample points equal to the length of the fibre divided by $2/3$. When the fibre is helical, the length of the fibre over 100 meters increases. The sample point is taken at $2/3$ m distance along the arc length of the fibre. So, $2/3$ m on the helical fibre is less than $2/3$ m on the straight fibre which means the helical fibre has more sample points than the straight fibre. While the amplitude is dampened in comparison to the straight fibre, the helical fibre provides more information about the 100 meters in our example than the straight fibre which also supports the use of helical fibre in seismic acquisition.

Full-waveform example

Now we combine the results of the P-wave and S-wave examples to study the effect that different gauge lengths have on the full-waveform response. We again repeat the experiment for saturated shale. We also only consider the vector $A = [0, 0, 1]$ as it produced the sharpest image for both straight and helical fibre. This example will only look at the response of the straight fibre. Over a distance of 100 m, we compare the following gauge lengths: 5 m, 10 m, 20 m and 25 m.

Fig. 8 shows the response of the straight fibre in shale for four different gauge lengths. The image is the sharpest for gauge length 5 m with the result for gauge length 10 m only slightly less sharp; however, we see a spreading of the hyperbola for gauge length 20 m and 25 m.

Recall that the gauge length considers the results of a small portion of the signal at a time, i.e., for our model: 5 m, 10 m, 20 m or 25 m. During that portion, gauge length is contracted or stretched depending on the shape of the signal. Since the response of the fibre is a hyperbolic, the larger gauge lengths contain a larger portion of the hyperbola. So, it holds more stretching and contracting information such that the two could cancel each other out as seen in the spreading of the hyperbolas in the results for gauge length 20 m and 25 m.

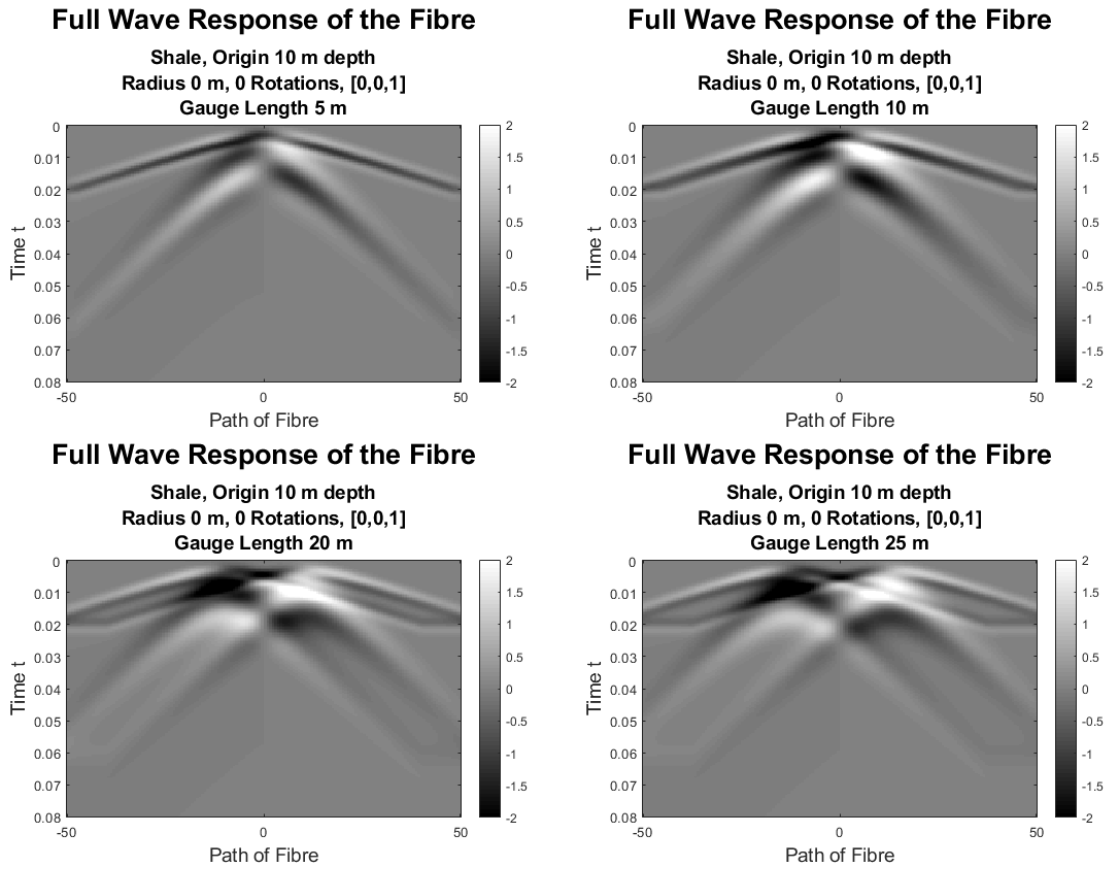

FIG. 8. The full-wave response of the straight fibre in saturated shale when A = [0,0,1] for (top left) Gauge length 5 m, (top right) Gauge length 10 m, (bottom left) Gauge length 20 m, and (bottom right) Gauge length 25 m

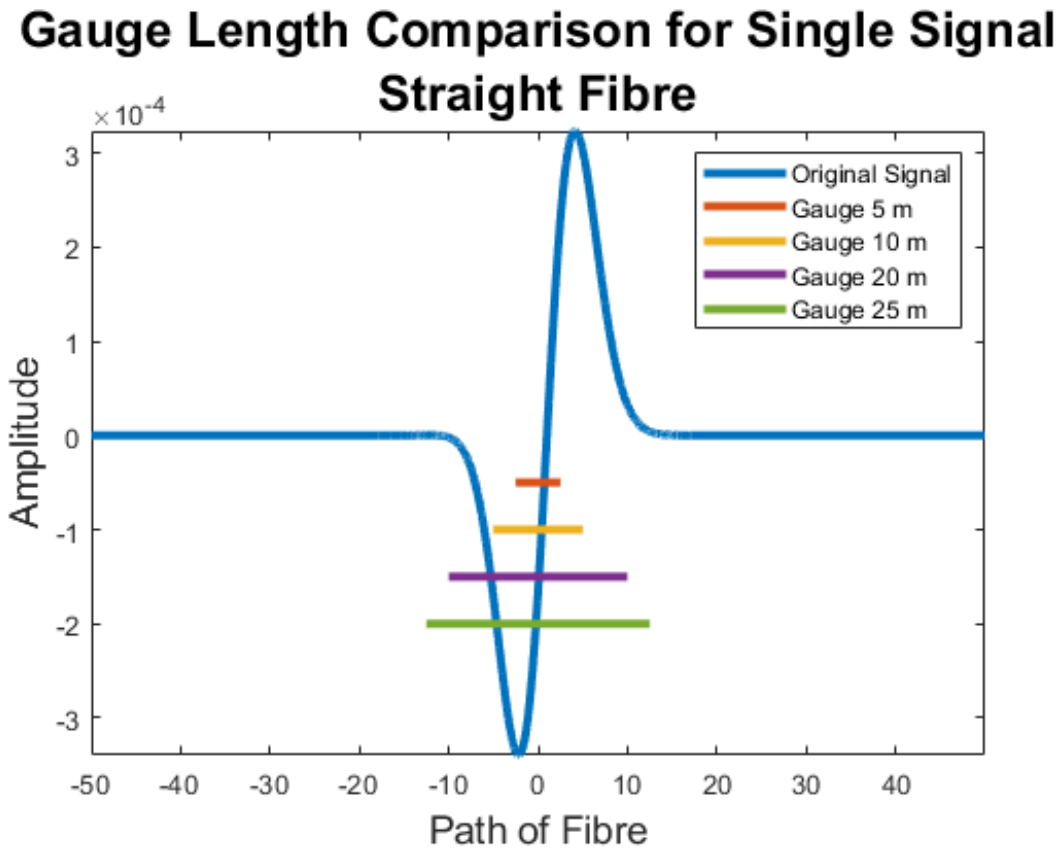

FIG. 9. Comparison of the gauge lengths with respect to the full-waveform signal at t_1 of the straight fibre: (Blue) Original signal at t_1 (Red) Gauge length 5m, (Yellow) Gauge length 10m, (Purple) Gauge length 20m, and (Green) Gauge length 25m.

Fig. 9 gives a physical representation of what we described in the previous paragraph. The gauge length 5 m only contains an increasing portion of the signal around the origin. The gauge length 10 m contains some decreasing signal but mostly increasing signal around the origin. Both gauge length 20 m and 25 m contain a lot of increasing and decreasing portions of the signal enough to cancel out the response at the origin which we see occurs in Fig. 10 for larger intervals around the origin as the gauge length increases.

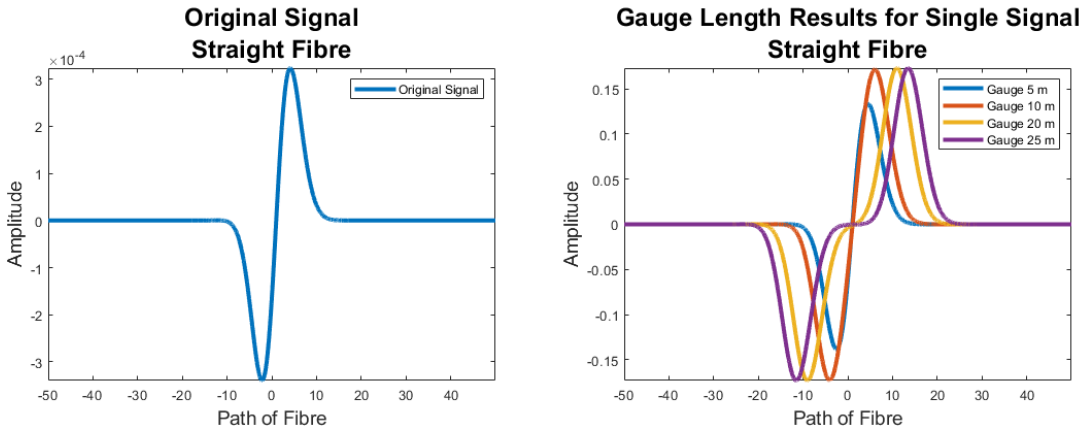

FIG. 10. (Left) The original signal at t_1 (Right) Comparison of the gauge lengths applied to the full-waveform signal at t_1 of the straight fibre: (Blue) Gauge length 5m, (Red) Gauge length 10m, (Yellow) Gauge length 20m, and (Purple) Gauge length 25m.

Fig. 10 only describes what occurs for the first time step t_1 of the full-waveform response of the straight fibre. It provides a good visual explanation for the spreading which occurs for the larger gauge lengths in the bottom two images of Fig. 8.

FUTURE WORK

This report contains an elementary study of an analytic model for DAS acquired seismic data. In the future, it would be beneficial to extend the analytic model to work for a varying velocity as opposed to a constant velocity. Given the solutions for reflection and transmission coefficients found in (Hardeman and Lamoureux, 2017), this extension seems achievable. We would also explore the response given a moving source instead of a stationary source. This investigation would help model seismic experiments involving ambient noise caused by vehicles or trains among other experiments. Also, we plan to study why the amplitude for the helical fibre's response is weaker than the straight fibre's response despite showing strain in more dimensions.

CONCLUSIONS

We began with an explanation of the model. We found the strain tensors for the P-wave, S-wave, and full-waveform responses. The results of the P-wave response in saturated shale and limestone were shown for straight fibre. Then, the S-wave response in saturated shale was explored for straight and helical fibre. We saw that the helical fibre detects strain in more dimensions than the straight fibre; however, the amplitude of the helical fibre's response was weaker in comparison to the straight fibre's response. Finally, we looked at the effects different gauge lengths had on the full-waveform response for straight fibre. The larger gauge lengths produced a spreading in the response which was not found in

the smaller gauge lengths. We noted that this is largely due to the amount of the signal contained in the larger gauge lengths which resulted in some cancellations.

ACKNOWLEDGEMENTS

We thank the sponsors of CREWES for their support. We also thank our collegues at Fotech as well as CREWES for their support. We also gratefully acknowledge support from NSERC (Natural Science and Engineering Research Council of Canada) through the grants CRDPJ 461179-13, CRDPJ 522863-17, and through a Discovery Grant for the second author.

REFERENCES

Aki, K., and Richards, P. G., 2002, Quantitative Seismology: University Science Books.

Bourbié, T., Coussy, O., and Zinszner, B., 1987, Acoustics of porous media: Editions Technip, Paris.

Eaid, M., Li, J., and Innanen, K., 2017, A coupled das shaped-fibre and 3d elastic finite difference wave model: CREWES Research Report, **29**, 1–19.

Hardeman, H. K., and Lamoureux, M. P., 2017, Accuracy of numerical solutions to the elastic wave equation in multiple dimensions: CREWES Research Report, **29**, 1–20.

Hartog, A. H., 2017, An introduction to distributed optical fibre sensors: CRC Press.